Electrical Modeling of Bifacial PV Modules

Preeti Kumari Sahu, Efstratios I. Batzelis, *Senior Member, IEEE,* Chandan Chakraborty, *Fellow, IEEE,* and J. N. Roy

***Abstract*—Although the bifacial photovoltaic (PV) module is now a mature technology, there still exists a gap in the literature on its electrical modeling and equivalent circuit representation. Most published studies have mainly focused on the photocurrent while overlooking other crucial parameters for the electrical response of the module. Even so, the photocurrent of the bifacial module is simplistically treated as the sum of individual currents of the front and rear sides, a hypothesis challenged in this study. Notably, our research has uncovered a discrepancy that can exceed 15%, and we address this issue by introducing a correction factor in this paper. This paper introduces a comprehensive electrical model that effectively integrates bifacial PV modules' front and rear sides into a single−circuit representation. This novel model adopts the single−diode equivalent circuit, formulating each of the five parameters as a function of the individual side's parameters. Indoor and outdoor measurements validate the accuracy improvement brought by this model, which can benefit energy yield studies and our theoretical understanding of bifacial PV systems.**

***Index Terms*—Bifacial, five−parameter model, photovoltaic, single−diode model,**

I. Introduction

THE renewable energy sector has witnessed a growing interest in the *bifacial* photovoltaic (PV) technology due to its increased energy yield potential [1]. Unlike the established *monofacial* PV modules that capture sunlight solely from their front side, bifacial PV modules utilize the light incident on the rear side as well, resulting in higher energy yield and efficiency. Studies have demonstrated that bifacial gain varies from 3.78% to 8.16%, and the tracker gain varies from 13.40% and 18.20% depending on weather conditions and system configuration, rendering this an appealing option for solar power generation [2].

While bifacial PV technology offers several benefits, there are also challenges related to design, installation, and operation that need to be addressed for its widespread adoption. One crucial aspect is the electrical equivalent circuit model for bifacial PV modules, which plays a significant role in optimizing their performance and predicting their behavior under different conditions. In 2019, the International Electrotechnical Commission (IEC) released a technical specification, known as IEC TS 60904−1−2 [3], to establish a standardized approach for evaluating the electrical output of bifacial PV modules. Although this specification introduces important macroscopic parameters such as the bifaciality factor, it does not make any recommendation on the circuit representation and the detailed electrical response of such modules. Such a model is much needed in many applications related to the design and operation of bifacial PV systems.

To meet this gap, recent studies have explored electrical models for bifacial PV modules and systems, centered around the single−diode equivalent circuit [4]–[16], which is an established model for monofacial modules. However, most of these papers focus only on the bifacial photocurrent, which is simplistically treated as the sum of the front and rear sides' photocurrents [6]–[9], [15], [16], an assumption shown in this paper to lead to errors of more than 15%. It is worth noting that this substantial error has not been widely acknowledged in the literature, possibly due to testing modules under sporadic conditions rather than a comprehensive investigation that sweeps through a wide range of front and rear contributions. Some studies represent the bifacial equivalent circuit as the two sides' circuits connected in parallel [14], [16], while others utilize empirical models without establishing a correlation between the front and rear sides of the bifacial PV module [4]. Another study employs both single and double-diode models for bifacial PV panels but does not establish specific relationships for the diode and shunt resistance parameters [15]. They assumed that both module sides have identical diode, shunt, and series resistances. However, our experimental findings demonstrate that these parameters differ between the two sides. These results underscore a significant gap in the modeling of individual parameters. In conclusion, the existing bifacial PV electrical models are not complete and are based on debatable assumptions.

To address this research gap, this paper proposes a new electrical model derived via 34 indoors and 25 outdoors experiments on a bifacial module at different illumination conditions ranging from (0−1000) W/m^2. This model adopts the single-diode equivalent and represents each of the five bifacial parameters as a function of the respective front and rear sides' parameters. Throughout the study, a P-type bifacial PV module (Adani, ASB−7−380) [17] is used, and the module specifications are detailed in Table I. Noteworthy outcomes from this investigation are:

1) It is found that the bifacial photocurrent is not simply the sum of two individual photocurrents as per the assumptions of most of the literature so far. There is a mismatch that varies up to more than 15%, which has been modeled via a correction factor,
2) A complete model for all five circuit parameters is introduced for the first time,
3) Experimental validation and comparison with the current state of the art demonstrates improvement of substantial modeling error.

The paper is organized into five different sections. Section II briefly reviews the single−diode model, the underlying physics, and existing bifacial PV models in the literature, while Section III delves into the development of the proposed model, offering insights into its formulation. The overall assessment

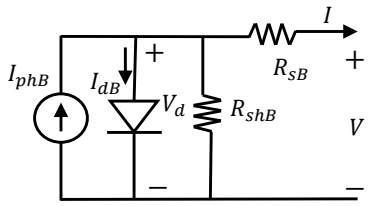

Fig. 1. Single−diode electrical equivalent circuit of the Bifacial PV cell.

of the proposed model, coupled with a detailed comparison with existing models, is expounded in Section IV. Finally, the overall conclusions are summarized in Section V.

II. Classical Single−Diode PV Model

A. Single−Diode Equivalent Circuit

The majority of relevant studies adopt the single-diode equivalent circuit to represent bifacial PV modules [4]–[16]. Although this model was first introduced and is still used for bifacial PV modules, this papers raises a concern about the lack of clarity regarding how the circuit parameters of the front and rear sides are interconnected within the model. The equivalent circuit shown in Fig. 1 involves a bifacial photocurrent source I_{phB}, the diode's saturation current I_{sB} and modified ideality factor α_B, and the series R_{sB} and shunt resistance R_{shB}. In this analysis, α_B represents the modified diode ideality factor, with units of 'V', and is expressed as shown in Eq. (2). Here, n is the standard diode ideality factor (dimensionless), and V_T represents the thermal voltage. The notation *B* signifies the parameters associated with the bifacial PV module.

The current-voltage equation of this model is given by

$$I = I_{phB} - I_{sB}\left(e^{\frac{V+IR_{sB}}{\alpha_B}} - 1\right) - \frac{V + IR_{sB}}{R_{shB}} \tag{1}$$

$$\alpha_B = nV_T \tag{2}$$

The premise of this paper is that this model can represent the electrical response of the bifacial module at all illumination conditions but with different parameters. Illuminating only the front side while keeping the rear surface in the dark, like a monofacial module, is referred to hereinafter as the *front* operating mode. Sole illumination of the rear side is denoted as the *rear* mode, and having both sides under the light as the *bifacial* mode. The model parameters at every mode differ, denoted as $\mathbf{P_x} = [I_{phx}, I_{sx}, a_x, R_{sx}, R_{shx}]$ where $x = F, R, B$ for front, rear and bifacial. The objective of this study is to establish a relation between these parameters $\mathbf{P_B} = f(\mathbf{P_F}, \mathbf{P_R})$ so as to quantify how the two sides are fused together into a combined bifacial response.

B. Underlying Physics

The operating principles of monofacial and bifacial PV technology share many similarities. In contrast to monofacial PV cells, bifacial PV cells are equipped with an anti−reflection coating and rear contacts [19]. Bifacial PV modules typically feature backsheet materials made of glass or transparent organic materials, each tailored to specific conditions.

In a bifacial PV module, electrons exhibit distinct behaviors when excited by photons originating from either the front or rear side. These behaviors are influenced by the module's unique design and intrinsic characteristics. A crucial concept in understanding the efficiency of carriers generated by light absorption in different regions of the device is the notion of *collection probability*. This probability depends on several key factors, such as the distance a light-generated carrier must travel relative to its diffusion length and the surface properties of the device.

Typically, the top surface layer (N−type) is about 1 μm thick, and the absorber layer (P−type) is approximately 100 μm thick. The N−type layer should ideally be very thin to ensure the depletion region is close to the surface. The thickness of P−type layer should be less than the minority carrier diffusion length to avoid recombination. An increase in thickness results in a higher short−circuit current density as more photons are absorbed, but it can decrease the open−circuit voltage (V_{oc}) due to increased recombination. Therefore, there is a trade−off, and the absorber layer thickness should ideally fall within a range of 50 to 100 μm.

In regions close to the p−n junction, known as the depletion region, the collection probability reaches its maximum value of unity. This is because the strong electric field in this region rapidly separates electron-hole pairs, ensuring their efficient collection as shown in Fig. 2. However, as we move away from the junction toward areas where carriers are generated farther from the junction, the collection probability significantly diminishes. When a carrier is generated beyond a distance equal to its diffusion length from the junction, the likelihood of its successful collection becomes notably low. Consequently, due to the varying distances between the surface (either rear or front) and the depletion region, the rear side is less efficient in this regard compared to the front side. This discrepancy is the underlying reason for the distinct behaviors exhibited by the front and rear sides of the bifacial module, even under the same irradiances conditions.

C. Existing Bifacial PV Models

Quite a few electrical models have been proposed in the literature to represent the behavior of bifacial PV modules [6]–[9], [15], [16], [20]. Most models focus on the photocurrent, in particular, [6]–[9], [16], [20], treating it as the sum of the two individual sides' photocurrents as in Eq. (3). In the

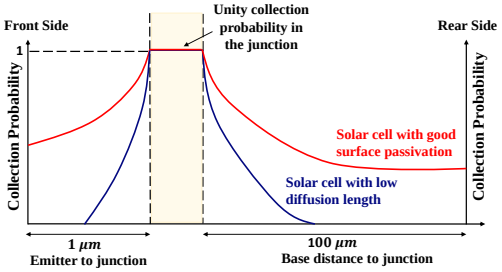

Fig. 2. Collection probablity of charge carriers in bifacial PV module [18].

study by [15], the electrical circuit model for the bifacial PV module was constructed using datasheet values at STC, whereas [20] relied solely on indoors measurements to develop their model for the same module. Although intuitive, this hypothesis is shown later and requires some adjustment for accurate representation.

$$I_{phB} = I_{phF} + I_{phR} \tag{3}$$

A modification to that equation is proposed in [6], where the contribution of either side is quantified via a coefficient β as in Eq. (4). Where, β is bifacial contribution rate. Still, this does not change the main premise of Eq. (3) (i.e. adding the two equations in Eq. (4) yields Eq. (3)).

$$\begin{aligned} I_{phF} &= \beta \times I_{phB} \\ I_{phR} &= (1-\beta) \times I_{phB} \end{aligned} \tag{4}$$

A different model proposed in [15] involves on all the parameters, but only the bifacial photocurrent (I_{ph}) and series resistance (R_s) are modeled separetely, whereas rest of the parameters are treated same as front side parameters. This model introduces β_{Isc}, which represents the bifaciality factor of the short circuit current, to modify the bifacial photocurrent by considering the difference in the short-circuit currents of the front and rear sides. Additionally, the model introduces β_{Isc} times an additional resistance term ($R_{add,SDM}$) to obtain the total series resistance of the bifacial PV module as shown in Eq. (5). The resistance $\beta_{Isc} \times R_{add,SDM}$ is added in series with R_s to compensate for the nonlinearity of the bifacial PV systems.

$$\begin{aligned} I_{phB} &= I_{phF}(1+\beta_{Isc}) \\ R_{sB} &= R_{sF} + \beta_{Isc} \times R_{add,SDM} \end{aligned} \tag{5}$$

The key takeaway from this review is that the majority of electrical models for bifacial PV systems have primarily focused on the photocurrent. In these models, the other four critical parameters have been typically assumed to be identical to the front side parameters, with only one study deviating from this norm by considering the series resistance as distinct and introducing an additional factor. Later in this paper we show that in fact all five front and rear parameters differ, which reveals on open gap in the literature. This underscores the pressing need for a more comprehensive electrical model that considers all circuit parameters.

III. Development of the Proposed Model

In this section, the methodology and essential steps involved in developing the proposed model are outlined. The study utilized a bifacial PV module (Adani, ASB−7−380) [17], and the module specifications are detailed in Table I. The experimental measurements conducted in this research involve two different test benches: an indoors solar simulator and an outdoors rooftop setup.

A. Indoor Measurements

The five parameters of the two sides are not identical at the same conditions (irradiance and temperature). This is confirmed by the indoor measurement test−sets as illustrated in Fig. 3. The solar simulator results shown in Fig. 3(a)−(e) illustrate how the individual sides' parameters vary with irradiance, allowing for a comparison between the front and rear sides' performance. It is worth noting that this test was not able to assess the bifacial operating mode.

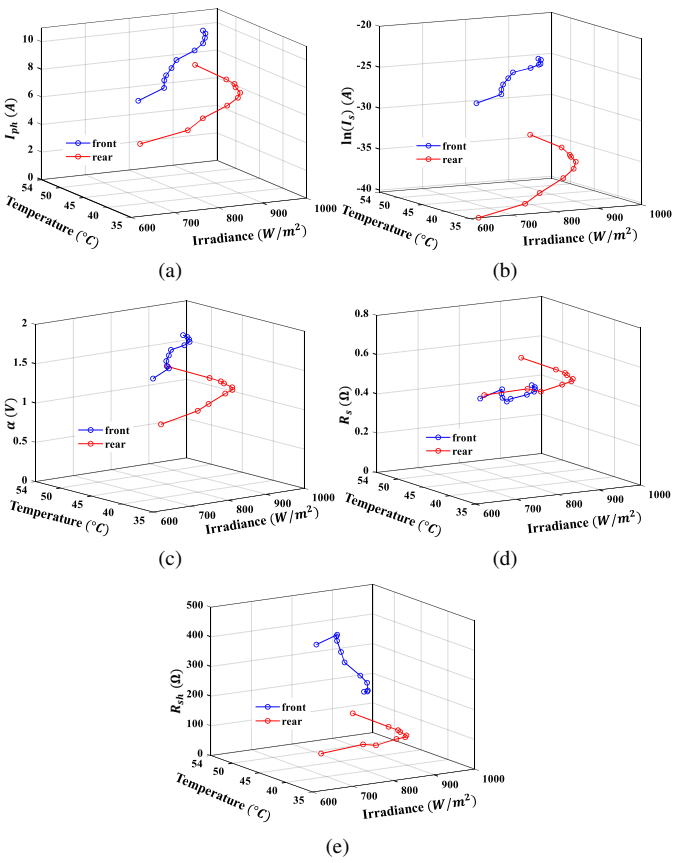

Fig. 3. Indoors results on the front and rear side parameters. (a) I_{ph}, (b) $ln(I_s)$, (c) α, (d) R_s and (e) R_{sh}.

It is important to note that during this test, both irradiance and temperature varied, as shown in Table I of the supplementary file. Consequently, these plots do not explicitly reflect the parameters' dependence on irradiance. Rather, they depict how the parameters differ between the two conditions under simultaneous changes in both irradiance and temperature.

Fig. 3(a) illustrates a strong positive correlation between the photocurrent I_{ph} produced by each module side and the incident irradiance, and a weaker temperature effect. As anticipated, the rear side yields a lower current compared to the front side under the same. This observation aligns with the expected

TABLE I
Specifications of the Bifacial PV Module under Test

Electrical Parameter	Front side	Both sides
Peak Power, P_{max} (W_p)	380	416
Maximum Voltage, V_{mpp} (V)	39.5	41.6
Maximum Current, I_{mpp} (A)	9.64	10.02
Open Circuit Voltage, V_{oc} (V)	47.77	48.14
Short circuit Current, I_{sc} (A)	10.11	11.02
Bifaciality factor for I_{sc}, ϕ_{Isc}	0.70	
Bifaciality factor for V_{oc}, ϕ_{Voc}	0.99	
Bifaciality factor for P_{max}, ϕ_{Pmax}	0.66	

behavior, as elucidated in the device physics discussion, where the efficiency of the rear side is acknowledged to be inferior to that of the front side in the bifacial PV module.

In Fig. 3(b)−(c), the two diode coefficients, I_s and a, demonstrate negligible irradiance dependence but a noteworthy positive correlation with temperature due to enhanced recombination at higher temperatures. It is worth noting that the rear side exhibits consistently lower diode parameters compared to the front side. Please note that the diode saturation current is treated in logarithmic form in Fig. 3(b) and elsewhere in this paper due to its variation by orders of magnitude.

The series resistance values of both sides in Fig. 3(d) are close to each other and near-constant. This indicates that R_s, which represents the resistance encountered by the current flow within the module, is not affected by irradiance or temperature similarly to monofacial modules. The two sides' series resistance is quite comparable, with no clear winner on this feature.

In contrast, the shunt resistance values depicted in Fig. 3(e) exhibit an inverse relationship with irradiance, for both sides. This means that the shunt resistance, which represents the undesired current paths or leakage paths in the module, becomes lower as the irradiance level rises which increases shunt losses, an observation reported for monofacial modules as well [21]. The rear side exhibits lower R_{sh} compared to the front side, indicating less efficient performance in consistence with the other parameters.

Using Indoors measurements, the bifaciality factors for I_{sc}, V_{oc}, and P_{max} were determined and are documented in the module specifications provided in Table I. A comprehensive analysis of the bifaciality factor of the module under investigation can be found in [22].

These findings reaffirm literature observations that the front side consistently outperforms the rear side under the same illumination conditions. Furthermore, they demonstrate that the parameters of two sides differ at the same conditions and therefore require separate modeling.

B. Outdoor Measurements

These tests study the model parameters extracted at the front, rear and bifacial operation at the same conditions aiming at modeling the correlation among them. The main objective is to understand how the front and rear contributions fuse into a combined bifacial output. It is useful to examine each parameter individually so that we get a deeper understanding of their significance and how they influence the electrical response of the module.

The following subsections adopt the concept of *normalized photocurrent* for the front and rear side, i_{phf} and i_{phr}, which refers to a relative measure of each side's contribution to the bifacial output as shown in Eq. (6).

$$i_{phf} = \frac{I_{phF}}{I_{phB}}, \qquad i_{phr} = \frac{I_{phR}}{I_{phB}} \tag{6}$$

1) Photocurrent (I_{ph}): Our hypothesis suggests that the region of the cell capable of being stimulated by both front- and rear-side irradiance may experience a missed opportunity

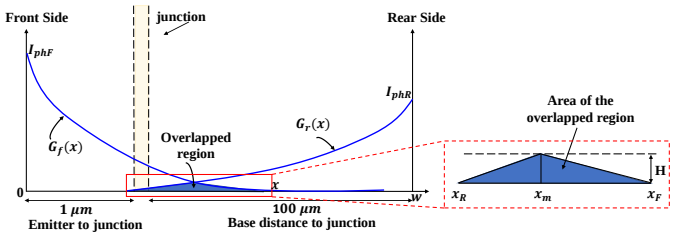

Fig. 4. Front and rear side photocurrent demonstration and area of the overlapped region

for current generation. This means that a single electron-hole pair could be created via either one or two incident photons. In essence, the bifacial collection probability is the combination of the front- and rear-side probabilities, subtracting the joint probability. The joint probability is illustrated in Fig. 4 as the overlapping region highlighted in blue. To determine the area of this overlapped region (denoted as γ), let us approximate it as a triangle, as shown in the zoomed version in Fig. 4.

The collection probability in conjunction with the generation rate in the solar cell determine the light-generated current from the solar cell. The light-generated current is the integration over the entire device thickness of the generation rate at a particular point in the device. Hence generation rate for front and rear sides are denoted as $G_f(x)$ and $G_r(x)$ respectively and are expressed as;

$$G_f(x) = J_{phF}\, e^{\left(\frac{-x}{\alpha}\right)} \tag{7}$$

$$G_r(x) = J_{phR}\, e^{\left(\frac{x-w}{\alpha}\right)} \tag{8}$$

where, J_{phF} and J_{phR} are the current density of front and rear side of the cell respectively. w is the thickness of cell, and x denoted as some portion of the cell thickness. α is the light absorption coefficient of the solar cell, typically $10^3/cm$ for Si. Assuming at x_F, the current density is 1% of H (height of the overlapped region as shown in Fig. 4), denoted as h_1. Similarly, at x_R, the current density is 1% of H, denoted as h_2. Let x_m be the intersection point of both front and rear side collection rates. To find the expression for x_F and x_R, the expression for H at x_m need to be evaluated. Hence;

$$\text{at} \quad x_m, \quad J_{phF}\, e^{\left(\frac{-x}{\alpha}\right)} = J_{phR}\, e^{\left(\frac{x-w}{\alpha}\right)} \longleftrightarrow$$

$$x_m = \frac{\alpha \ln\left[\frac{J_{phF}}{J_{phR}}\right] + w}{2} \tag{9}$$

Therefore the expression of H can be written as shown in Eq. (10).

$$H = J_{phF}\, e^{\left(\frac{-x_m}{\alpha}\right)} \longleftrightarrow$$

$$H = \sqrt{J_{phF} J_{phR}}\left(e^{\left(\frac{-w}{2\alpha}\right)}\right) \tag{10}$$

Hence the expression for x_F and x_R can be shown as in Eqs. (11) and (12).

$$x_F = \frac{w}{2} - \alpha \ln\left[0.01\sqrt{\frac{J_{phR}}{J_{phF}}}\right] \tag{11}$$

$$x_R = \frac{w}{2} + \alpha \ln\left[0.01\sqrt{\frac{J_{phF}}{J_{phR}}}\right] \tag{12}$$

Now, the area of the overlapped region can be expressed as;

$$\begin{aligned}\gamma &= \frac{1}{2} \times H \times (x_F - x_R) \longleftrightarrow \\ &= \frac{1}{2} \times \sqrt{J_{phF} J_{phR}} \left(e^{\left(\frac{-w}{2\alpha}\right)} \right) \times (x_F - x_R) \\ &\approx \sqrt{J_{phF} J_{phR}} \end{aligned} \tag{13}$$

First order Taylor series approximation of $\sqrt{x+1}$ around $x = 0 \Rightarrow 1 + \frac{x}{2}$. Hence Eq. (13) can be rewritten as $\sqrt{(J_{phF} J_{phR} - 1) + 1}$. Therefore the first order Taylor series approximation of Eq. (13) resulting in;

$$\gamma = \frac{J_{phF} J_{phR} + 1}{2} \approx \frac{J_{phF} J_{phR}}{2}, \quad \text{as} \quad J_{phF} J_{phR} >> 1 \tag{14}$$

For our simplicity we convert the γ into pu value, then Eq. (14) is resulting in;

$$\gamma_{pu} = \frac{j_{phf} j_{phr}}{2} (J_{phF} + J_{phR}) \tag{15}$$

Therefore the photocurrent J_{phB} can be expressed as;

$$J_{phB} = (J_{phF} + J_{phR}) \left[1 - \frac{j_{phf} j_{phr}}{2} \right] \tag{16}$$

where, j_{phf} and j_{phr} are the pu (per unit) current density of front and rear side of the cell respectively. The bifacial photocurrent expression can be obtained by integrating Eq. (16) over 0 to w;

$$I_{phB} = (I_{phF} + I_{phR}) \left[1 - \frac{i_{phf} i_{phr}}{2} \right] \tag{17}$$

Fig. 5(a) depicts the photocurrent in the three operating modes (front, rear, bifacial) extracted from the measurements represented by blue, red and green line respectively, alongside benchmark1$-$2 as given in Table II based on the Eq. (3) hypothesis (purple line), plotted against i_{phf}. The front and rear sides' photocurrents vary from zero to their maximum value, so as to capture a wide range of operating conditions with different levels of either side's contribution to the bifacial output.

It is worth noting that the marginal i_{phf} values of 1 and 0, referring to 0° and 180° tilt respectively, do not correspond to maximum photocurrent generation. The front-side photocurrent gets maximum at about 22° and the rear-side photocurrent at 140° when the incident irradiance is maximised, hence the non-monotonic trend of blue and red lines in Fig. 5(a).

Comparing measured and benchmark1$-$2 bifacial current, it is evident that there is a mismatch for intermediate i_{phf} values. This mismatch is plotted separately in Fig. 5(b) (blue line), indicating that when one side is illuminated much more than the other (i_{phf} close to 0 or 1) the mismatch is negligible;

TABLE II
BENCHMARK BIFACIAL PV MODELS

Parameters	benchmark1	benchmark2
I_{phB}	$I_{phF} + I_{phR}$	
I_{sB}	I_{sF}	I_{sR}
a_B	a_F	a_R
R_{sB}	R_{sF}	R_{sR}
R_{shB}	R_{shF}	R_{shR}

however, when both sides are under light, this mismatch takes values up to 18%. This is an important observation made for the first time, which indicates that the two sides do not work independently but one affects the other. This validate our hypothesis Eq. (17).

Fig. 5(b) shows that modeling of this mismatch by γ demonstrates good agreement with the measured values. It is important to note that the γ is zero when only one side is illuminated. However, when both sides are active it takes positive values and gets maximum when the two sides contribute comparably, as clearly depicted in Fig. 5(b). As a result, the proposed model provides a more accurate estimation of I_{phB} in Fig. 5(a) (black line), compared to benchmark1$-$2 and existing literature.

For further illustration, we varied the irradiance from 600 to 1000 W/m^2, keeping the tilt angle constant over a period of time. We measured three modes and conducted a comparison of the proposed model with the benchmark model, as depicted in Fig. 5(c). It is evident that both front side and rear side photocurrents increase with an increase in irradiance, which reaffirm indoor measurement study. However, the bifacial photocurrent does not simply sum up the photocurrents from the two sides; rather, it aligns closely with the proposed model, demonstrating good accuracy.

2) Diode parameters (I_s and a): Fig. 5(e) and (f) illustrate the two diode parameters I_s and a as extracted in the front, rear, and bifacial modes plotted against incident irradiance to have a clear picture. These plots reaffirm the observations of indoor experiments on the different front and rear values (in Fig. 3(b)-(c)), but more importantly, show that the bifacial parameters (green line) seem to be a weighted average of the two sides. This observation, reported for the first time in this paper, indicates that there is a relation between the bifacial and the two sides' diode parameters that is yet to be identified.

To approximate this relation, the diode current I_d (see Fig. 1) is used as a starting point. Fig. 5(d) shows an example from the outdoor measurements of the diode currents for the front I_{dF}, rear I_{dR} and bifacial I_{dB} modes (circle markers). It is apparent that I_{dB} lies within I_{dF} and I_{dR}, and in fact it can be reasonably approximated as a weighted average of the two using the normalized photocurrents as weights (black line):

$$I_{dB} = i_{phf} I_{dF} + i_{phr} I_{dR} \tag{18}$$

Substituting the diode parameters in this equation and some manipulation yields:

$$\begin{aligned} & I_{sB} e^{\frac{V_d}{a_B}} = i_{phf} I_{sF} e^{\frac{V_d}{a_F}} + i_{phr} I_{sR} e^{\frac{V_d}{a_R}} \longleftrightarrow \\ & 1 = i_{phf} \frac{I_{sF}}{I_{sB}} e^{V_d \left(\frac{1}{a_F} - \frac{1}{a_B}\right)} + i_{phr} \frac{I_{sR}}{I_{sB}} e^{V_d \left(\frac{1}{a_R} - \frac{1}{a_B}\right)} \end{aligned} \tag{19}$$

It is easy to see that the exponential terms in Eq. (19) are close to 1 as their exponents are close to 0, which allows for

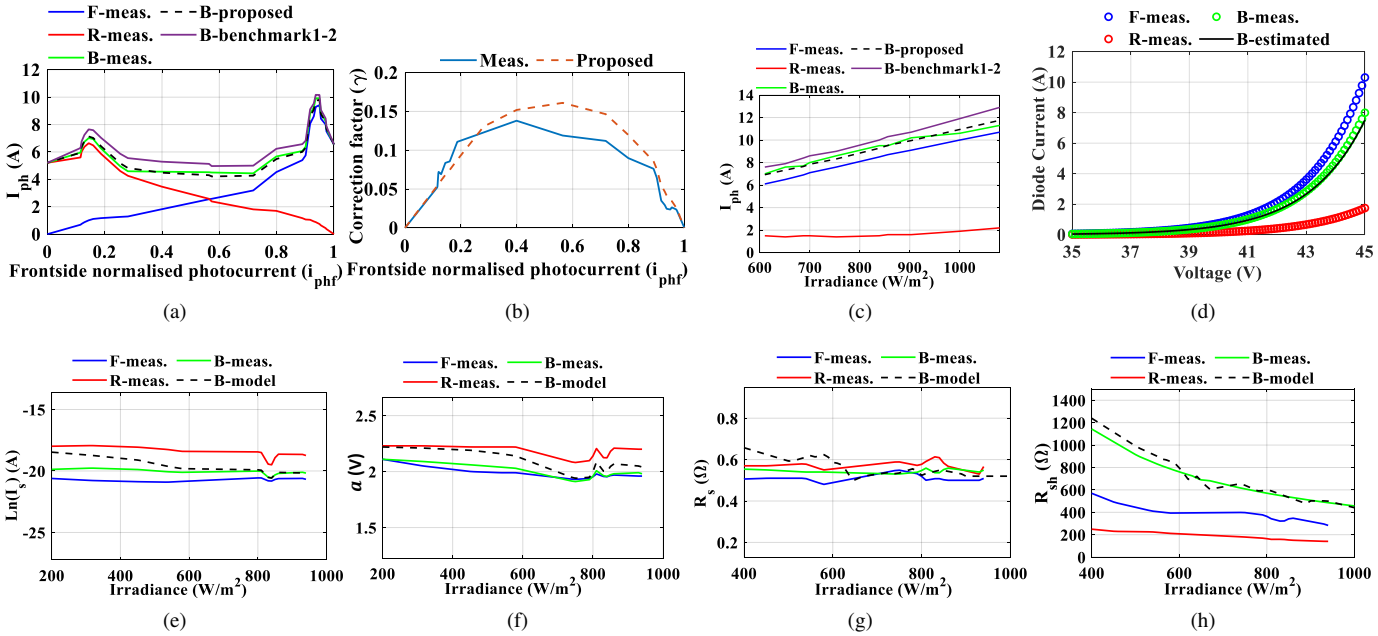

Fig. 5. Outdoors measurements modeled and measured: (a) photocurrent (I_{ph}), (b) Mismatch and correction factor (γ), (c) photocurrent vs. irradiance, (d) Diode current, (e) saturation current in logarithmic scale ($ln(I_s)$), (f) modified diode ideality factor (a), (g) series resistances (R_s), and (h) shunt resistances (R_{sh})

first−order Taylor series approximation around 0 resulting in:

$$\begin{aligned} 1 = & i_{phf}\frac{I_{sF}}{I_{sB}}\left[1+V_d\left(\frac{1}{a_F}-\frac{1}{a_B}\right)\right] \\ & + i_{phr}\frac{I_{sR}}{I_{sB}}\left[1+V_d\left(\frac{1}{a_R}-\frac{1}{a_B}\right)\right] \longleftrightarrow \\ 1 = & \frac{i_{phf}I_{sF}+i_{phr}I_{sR}}{I_{sB}} \\ & + V_d\left[i_{phf}\frac{I_{sF}}{I_{sB}}\left(\frac{1}{a_F}-\frac{1}{a_B}\right)+i_{phr}\frac{I_{sR}}{I_{sB}}\left(\frac{1}{a_R}-\frac{1}{a_B}\right)\right] \end{aligned} \tag{20}$$

$$I_{sB} = i_{phf}I_{sF} + i_{phr}I_{sR} \tag{21}$$

$$a_B = \frac{i_{phf}I_{sF}+i_{phr}I_{sR}}{i_{phf}\frac{I_{sF}}{a_F}+i_{phr}\frac{I_{sR}}{a_R}} \tag{22}$$

For Eq. (20) to hold true at any voltage V_d, two conditions must be satisfied: the first term on the right-hand side should be equal to 1, and the second term multiplying the voltage should be equal to 0. This observation leads to Eq. (21)−(22), formulating the two bifacial diode parameters as explicit functions of the front and rear sides' parameters weighted on the respective normalized photocurrents. The proposed model shown in black lines in Fig. 5(e) and Fig. 5(f) follows the same trend as the measured values but with some noteworthy deviation. Despite the limitations, this model clearly outperforms the approach of assuming only the front side (benchmark1) or rear side (benchmark2) parameters.

3) Resistance parameters (R_s and R_{sh}): Fig. 5(g) and (h) depicts the comparison between the measured and modeled values of the two resistances. In Fig. 5(g), the bifacial series resistance (R_s) undergoes measurement across a broad range of irradiances. R_s appears to remain nearly constant, exhibiting minimal variation with irradiance levels. Some deviations observed at certain irradiances can be attributed to measurement errors. The modeling of the R_s involves considering both front and rear side resistances as shown in Fig. 5(g), suggesting it is a weighted average of the two.

Adding rear side contact material to a solar PV cell structure can have implications for the series resistance. The series resistance in a solar PV cell primarily consists of the resistance of the semiconductor material itself and the resistance of the metal contacts (both front and rear). When rear side contact material is added, it provides an additional conductive path for the current generated in the cell to flow out, reducing the overall series resistance. This is because the rear side contact reduces the distance the charge carriers (electrons and holes) have to travel to reach the contacts, thus lowering the resistive losses. Therefore, the addition of rear side contact material typically leads to a decrease in the series resistance of the bifacial PV cell structure. The modeled resistance is then compared with the measured values, as illustrated in Fig. 5(g).

Conversely, shunt resistance (R_{sh}) appears to be inversely proportional to irradiance as shown in Fig. 5(h). As irradiance levels rise, the R_{sh} of the bifacial PV system decreases. This phenomenon is attributed to the increased photon generation with higher irradiance, causing more recombination within the cell and consequently leading to a decrease in R_{sh}. By examining the R_{sh} of the front and rear sides, it is evident that the overall R_{sh} can be modeled as a simple summation of the two sides. This could be due to the following reasons:

- Optimized Cell Design: Bifacial PV cell manufacturers may incorporate design improvements to minimize defects and enhance electrical properties, resulting in increased shunt resistance,
- Improved Cell Quality: Higher quality materials and

manufacturing processes can lead to reduced defects and improved electrical characteristics, including higher shunt resistance,

- Optimized Bifacial Operation: Bifacial PV cells may be designed or operated in a way that minimizes shading and maximizes light exposure on both the front and rear sides, reducing localized shunt currents and increasing shunt resistance.

The modeled R_{sh} is then compared with the measured values, as depicted in Fig. 5(h). Based on these observations, we can develop a simple model for R_s and R_{sh} as in Eq. (23)−(24). Both R_{sB} and R_{shB} approximation in Fig. 5(g) and (h) are of very good accuracy. Both the resistances reaffirm the study done in indoor measurements.

$$R_{sB} = i_{phf} R_{sF} + i_{phr} R_{sR} \tag{23}$$

$$R_{shB} = R_{shF} + R_{shR} \tag{24}$$

Therefore in the proposed model, we utilize the single−diode circuit, and each of the bifacial parameters is expressed as a function of the corresponding parameters for the front and rear sides of the module as depicted in Fig. 6. The equations representing this model are provided in Eqs. (17) and (21)–(24). This approach enables a more comprehensive and accurate representation of the electrical behavior of bifacial PV modules. It is worth noting that these equations are derived on the investigated module. Future work will validate and expand this model across several bifacial modules.

It is worth noting that, similar to the indoor tests, both irradiance and temperature vary in Fig. 5(c), (e)-(h) according to Table II of the supplementary file. Consequently, these plots do not explicitly reflect the effect of irradiance on these parameters.

IV. Overall Assessment

This section assesses the overall performance of the proposed model over the alternative benchmark1−2 derived from the literature as shown in Table II. To assess the performance of these models in all regards, three different error metrics are employed: (i) the parameter estimation error E_{rms}, (ii) the curve deviation D_{rms}, and (iii) MPP power deviation P_{err}. These metrics indicate how well the models represent the individual parameters, the entire I−V curve and the maximum power respectively, and are all equally important for a holistic assessment of performance.

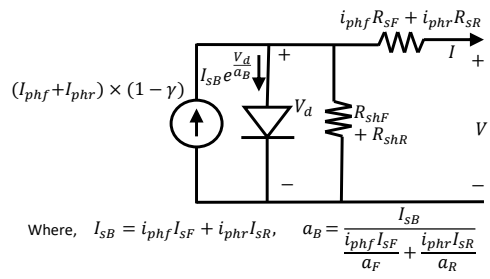

Fig. 6. Proposed single-diode electrical equivalent circuit of the bifacial PV cell.

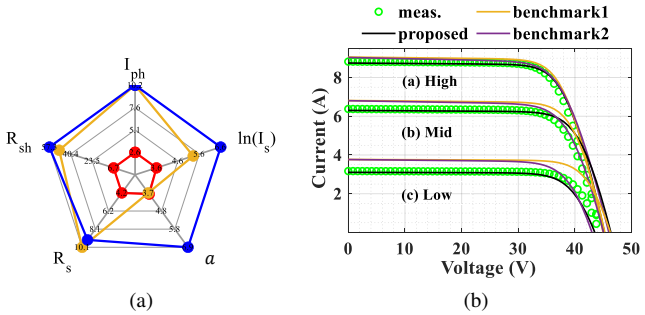

(a) (b)

Fig. 7. (a) Spider graph of the RMS estimation errors (%) (Proposed in red, Benchmark1 in orange, Benchmark2 in blue), (b) Measured and reconstructed I−V curves for three instances of (a) high, (b) medium, (c) and low irradiance.

TABLE III
RMS and MAX Errors in Estimating the Five Model Parameters

Five Parameters	RMS Error (%)			MAX Error (%)		
	Model	Bmrk1	Bmrk2	Model	Bmrk1	Bmrk2
I_{ph}	*2.6*	10.2	10.2	*6.4*	20.9	20.9
$ln(I_s)$	*3.6*	5.3	6.6	*8.6*	9.9	10.2
a	3.8	*3.7*	6.9	*6.1*	7.7	11.6
R_s	*4.2*	10.1	9.3	*8.9*	21.6	23.5
R_{sh}	*6.7*	49.6	57.3	*12.3*	72.9	69.0

*Bmrk1−2: Benchmark1−2

The parameters estimation is evaluated via the metrics of RMS error E_{rms} and maximum error E_{max} across all 25 outdoor measurements as shown in Eqs. (25) and (26), where X_{meas} and X_{est} are the measured and estimated values for every parameter X.

$$E_{rms} = rms\left(\frac{X_{est} - X_{meas}}{X_{meas}}\right) \tag{25}$$

$$E_{max} = max\left(\frac{X_{est} - X_{meas}}{X_{meas}}\right) \tag{26}$$

The results are tabulated in Table III, where italic font indicates the lowest error. It is apparent that the proposed model demonstrates the most favorable accuracy, particularly in estimating the crucial parameter of photocurrent. The model achieves significantly lower errors in I_{ph}, about three to four times less than the benchmarks. More importantly, our model maintains reliable estimations across all parameters, with RMS errors consistently below 7% and MAX errors marginally exceeding 12%, as opposed to more than 50% and 70% respectively in the benchmarks. These observations are further consolidated in the spider graph of Fig. 7(a), which illustrates the multi−faceted superiority of the proposed model against the literature.

The next step is to assess how the parameter estimation translates to an accurate I−V curve representation, which is the end result. Fig. 7(b) shows three such measured curves at representative low, medium, and high irradiances (circle markers), alongside the modeled curves via the three approaches. High irradiances corresponds to levels nearing (800−1000) W/m^2, while medium irradiances encompass the range between (500−800) W/m^2, and low irradiances signify values between (100−500) W/m^2. It is evident that the proposed model matches better the measured values, especially in the short circuit region (horizontal part) due to the improved

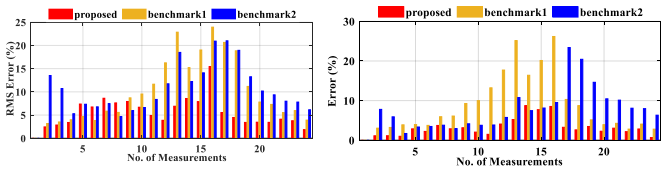

(a) (b)

Fig. 8. (a) Curve deviation between measured and modeled I−V curves via the three models, (b) Power deviation analysis

modeling of I_{ph}. To evaluate the overall performance in the I−V curve representation, the curve deviation metric is adopted:

$$D_{rms} = rms\left(\frac{I_{est} - I_{meas}}{I_{mpp,meas}}\right) \tag{27}$$

where I_{est} and I_{meas} are the estimated and measured currents, respectively, while $I_{mpp,meas}$ is the measured Maximum Power Point current. The latter is used for normalization purposes. These results are visualized in Fig. 8(a) for all 25 measurements and three models. It is apparent that the proposed model demonstrates consistently lower errors, exhibiting overall about 7% RMS curve deviation for all scenarios, as opposed to 12.3% and 11.9% of benchmark 1 and 2 respectively. This reaffirms that the derived model has established a valid formulation of how the front and rear sides interact to produce a combined bifacial response.

To further assess performance, power analysis is conducted, comparing the proposed model with benchmark1-2, as illustrated in Fig. 8(b). The MPP power deviation is evaluated via a metric of error, P_{err} across all 25 outdoor measurements as shown in Eq. (28), where $P_{mpp,est}$ and $P_{mpp,meas}$ are the estimated and measured power at Maximum Power Point respectively.

$$P_{err} = \frac{P_{mpp,est} - P_{mpp,meas}}{P_{mpp,meas}} \tag{28}$$

The results reveal that the proposed model demonstrates a RMS power deviation of 3.9%. In contrast, the benchmark models show significantly higher deviations, with benchmark 1 exhibiting an RMS power deviation of 11.3% and benchmark 2 showing a deviation of 9.4%. This comparison highlights the superior accuracy of the proposed model in estimating power at the MPP under various outdoor conditions.

To clarify which parameter most significantly contributes to the reduction of P_{err}, we performed a correlation analysis between each parameter and the overall curve deviation errors. The correlation coefficients between each parameter and the overall error were calculated to determine their influence on reducing P_{err} as shown in Fig. 9. The correlation of P_{err} with all five parameter errors falls within the range of 20–30%, indicating that all parameters have a comparable influence on the overall electric response. Some parameters show high correlation with each other, suggesting simultaneous modeling mistakes and identifying areas where further improvements could be made.

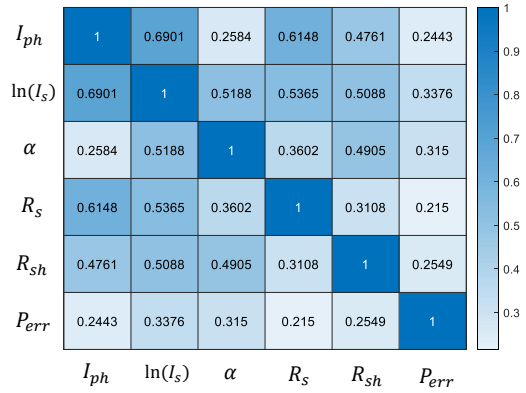

Fig. 9. Correlation coefficients between each parameter and the overall power deviation (P_{err}).

V. Conclusion

This paper mainly focuses on the development of the complete electrical modeling of the bifacial PV module. The widely adopted single−diode model for monofacial PV modules is applied to the bifacial PV module in this study. However, the current methodology of simply adding front and rear side photocurrents of the bifacial PV module, leads to a mismatch that gets maximum, when both sides are illuminated differently and may exceed 15%. Motivated by this discrepancy, the paper delves into the physics behind the bifacial PV system. Leveraging the concept of collection probability, a novel photocurrent model is developed. Furthermore, the diode parameters are determined as the weighted average of those from both sides. Despite the expectation for bifacial shunt resistance to be connected in parallel, experimental findings reveal a series connection. This unexpected outcome is attributed to the optimized cell design, and improved quality of bifacial cells. Similarly, the series resistance is computed as the weighted average of the resistances from both sides. These observations culminate in a complete electrical model for bifacial modules, demonstrating superior performance in parameter estimation and I−V curve representation compared to existing alternatives. Notably, the proposed model is experimentally validated and it has demonstrated lower errors with an overall about 7% RMS curve deviation for all scenarios, compared to the RMS error ranging from 11.9% to 12.3% observed in existing models.

Future work will explore extending our model to additional bifacial panels and employ different parameter extraction algorithms to further enhance its accuracy and reliability.

Acknowledgment

This work was financially supported by the Department of Science and Technology (DST), India, and the European Union's Horizon 2020 Research and Innovation Program through the RE-EMPOWERED Project under Grant Agreement No DST/TMD/INDIA/EU/ILES/2020/50(c) and 101018420 respectively, as well as by the UNIFORM project supported by UKRI under Grant agreement EP/Y001575/1 and the RAEng under the Engineering for Development Research Fellowship scheme (number RF/201819/18/86). For the

purpose of open access, the author has applied a Creative Commons attribution license (CC BY) to any Author Accepted Manuscript version arising from this submission.

REFERENCES

[1] IEA, "Renewable electricity growth is accelerating faster than ever worldwide, supporting the emergence of the new global energy economy," *News*, pp. p–1, 2021.

[2] K. B. de Melo, M. K. da Silva, J. L. de Souza Silva, T. S. Costa, and M. G. Villalva, "Study of energy improvement with the insertion of bifacial modules and solar trackers in photovoltaic installations in brazil," *Renewable Energy Focus*, vol. 41, pp. 179–187, 2022.

[3] I. P. Devices-Part, "Part 1–2: Measurement of current-voltage characteristics of bifacial photovoltaic (pv) devices," *IEC TS*, pp. 60 904–1, 2019.

[4] S. Bouchakour, D. Valencia-Caballero, A. Luna, E. Roman, E. A. K. Boudjelthia, and P. Rodríguez, "Modelling and simulation of bifacial pv production using monofacial electrical models," *Energies*, vol. 14, no. 14, p. 4224, 2021.

[5] W. Gu, T. Ma, M. Li, L. Shen, and Y. Zhang, "A coupled optical-electrical-thermal model of the bifacial photovoltaic module," *Applied Energy*, vol. 258, p. 114075, 2020.

[6] D. Hong, J. Ma, K. L. Man, H. Wen, and P. Wong, "Prediction of iv characteristics for bifacial pv modules via an alpha-beta single double-diode model," in *2022 IEEE Energy Conversion Congress and Exposition (ECCE)*. IEEE, 2022, pp. 1–5.

[7] E. Mouhib, L. Micheli, F. M. Almonacid, and E. F. Fernández, "Overview of the fundamentals and applications of bifacial photovoltaic technology: Agrivoltaics and aquavoltaics," *Energies*, vol. 15, no. 23, p. 8777, 2022.

[8] G. Raina, S. Mathur, and S. Sinha, "Behavior of bifacial and monofacial photovoltaic modules under partial shading scenarios," *International Journal of Energy Research*, vol. 46, no. 9, pp. 12 837–12 853, 2022.

[9] G. Raina and S. Sinha, "A comprehensive assessment of electrical performance and mismatch losses in bifacial pv module under different front and rear side shading scenarios," *Energy Conversion and Management*, vol. 261, p. 115668, 2022.

[10] J. Johnson, D. Yoon, and Y. Baghzouz, "Modeling and analysis of a bifacial grid-connected photovoltaic system," in *2012 IEEE Power and Energy Society General Meeting*. IEEE, 2012, pp. 1–6.

[11] Y. Tao, J. Bai, R. K. Pachauri, Y. Wang, J. Li, and H. K. Attaher, "Parameterizing mismatch loss in bifacial photovoltaic modules with global deployment: A comprehensive study," *Applied Energy*, vol. 303, p. 117636, 2021.

[12] Y. Zhang, Q. Gao, Y. Yu, and Z. Liu, "Comparison of double-side and equivalent single-side illumination methods for measuring the i–v characteristics of bifacial photovoltaic devices," *IEEE Journal of Photovoltaics*, vol. 8, no. 2, pp. 397–403, 2018.

[13] R. Castro and M. Silva, "Experimental and theoretical validation of one diode and three parameters–based pv models," *Energies*, vol. 14, no. 8, p. 2140, 2021.

[14] O. Hachana, B. Aoufi, G. M. Tina, and M. A. Sid, "Photovoltaic mono and bifacial module/string electrical model parameters identification and validation based on a new differential evolution bee colony optimizer," *Energy Conversion and Management*, vol. 248, p. 114667, 2021.

[15] E. M. Ahmed, M. Aly, M. Mostafa, H. Rezk, H. Alnuman, and W. Alhosaini, "An accurate model for bifacial photovoltaic panels," *Sustainability*, vol. 15, no. 1, p. 509, 2023.

[16] B. G. Bhang, W. Lee, G. G. Kim, J. H. Choi, S. Y. Park, and H.-K. Ahn, "Power performance of bifacial c-si pv modules with different shading ratios," *IEEE Journal of Photovoltaics*, vol. 9, no. 5, pp. 1413–1420, 2019.

[17] "Bifacial PV datasheet," October 2022. [Online]. Available: https://www.adanisolar.com/-/media/Project/AdaniSolar/Media/Downloads/Downloads/Corporate/Adani-Solar-E-Folder-Worldwide.pdf

[18] C. Honsberg and S. G. Bowden, "Photovoltaics education website," *PV Education*, 2019.

[19] W. Gu, T. Ma, S. Ahmed, Y. Zhang, and J. Peng, "A comprehensive review and outlook of bifacial photovoltaic (bpv) technology," *Energy Conversion and Management*, vol. 223, p. 113283, 2020.

[20] J. P. Singh, A. G. Aberle, and T. M. Walsh, "Electrical characterization method for bifacial photovoltaic modules," *Solar energy materials and solar cells*, vol. 127, pp. 136–142, 2014.

[21] M. K. da Silva, M. S. Gul, and H. Chaudhry, "Review on the sources of power loss in monofacial and bifacial photovoltaic technologies," *Energies*, vol. 14, no. 23, p. 7935, 2021.

[22] P. K. Sahu, E. I. Batzelis, J. Roy, and C. Chakraborty, "Irradiance effect on the bifaciality factors of bifacial pv modules," in *2022 IEEE 1st Industrial Electronics Society Annual On-Line Conference (ONCON)*. IEEE, 2022, pp. 1–6.